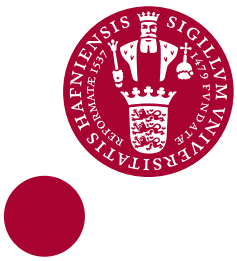

UV-vis Imaging of Piroxicam Supersaturation, Precipitation, and Dissolution in a Flow-Through Setup

Sun, Yu; Chapman, Alex; Larsen, Susan W.; Jensen, Henrik; Petersen, Nickolaj J.; Goodall, David M.; Ostergaard, Jesper

Published in:
Analytical Chemistry

DOI:
10.1021/acs.analchem.8b00587

Publication date:
2018

Document version
Peer reviewed version

UV-vis imaging of piroxicam supersaturation, precipitation and dissolution in a flow-through setup

Sun, Y., Chapman, A., Larsen, S. W., Jensen, H., Petersen, N. J., Goodall, D. M., & Østergaard, J.

Published in:
Analytical Chemistry

DOI:
10.1021/acs.analchem.8b00587

Publication date:
2018

Document version:
Peer reviewed version

Citation for published version (APA):
Sun, Y., Chapman, A., Larsen, S. W., Jensen, H., Petersen, N. J., Goodall, D. M., & Østergaard, J. UV-vis imaging of piroxicam supersaturation, precipitation and dissolution in a flow-through setup. Anal. Chem. 90, 6413-6418. 2018. https://doi.org/10.1021/acs.analchem.8b00587

UV-Vis Imaging of Piroxicam Supersaturation, Precipitation and Dissolution in a Flow-Through Setup

Yu Sun†, Alex Chapman‡, Susan W. Larsen†, Henrik Jensen†, Nickolaj J. Petersen†, David M. Goodall‡, and Jesper Østergaard†,*

†Department of Pharmacy, Faculty of Health and Medical Sciences, University of Copenhagen, Universitetsparken 2, DK-2100 Copenhagen Ø, Denmark.

‡ Paraytec Limited, York House, Outgang Lane, Osbaldwick, YO195UP, United Kingdom.

ABSTRACT: Evaluation of drug precipitation is important in order to address challenges regarding low and variable bioavailability of poorly water-soluble drugs, to assess potential risk of patient safety with infusion therapy and to explore injectable in situ suspension-forming drug delivery systems. Generally, drug precipitation is assessed in vitro through solution concentration analysis methods. Dual-wavelength UV-Vis imaging is a novel imaging technique which may provide an opportunity for simultaneously monitoring changes in both solution and solid phases during precipitation. In the present study, a multimodal approach integrating UV-Vis imaging, light microscopy and Raman spectroscopy was developed for characterization of piroxicam supersaturation, precipitation and dissolution in a flow-through setup. A solution of piroxicam dissolved in 1-methyl-2-pyrrolidinone was injected into a flowing aqueous environment (pH 7.4), causing piroxicam to precipitate. Imaging at 405 and 280 nm monitored piroxicam concentration distributions during precipitation and revealed different supersaturation levels dependent on the initial concentration of the piroxicam solution. The combination with imaging at 525 nm, light microscopy and Raman spectroscopy measurements demonstrated concentration-dependent precipitation and the formation, growth, and dissolution of individual particles. Results emphasize the importance of the specific hydrodynamic conditions on the piroxicam precipitation. The approach used may facilitate comprehensive understanding of drug precipitation and dissolution processes and may be developed further into a basic tool for formulation screening and development.

The amount of drug substance encountered in the circulatory system after injection or oral administration is often closely related to the ability of the substance to enter into and sustain a solution. After intravenous injection, precipitation of the drug may be associated with pain, inflammation and possibly reduced bioavailability.[1] However, the formation of a drug particle suspension upon injection, e.g., subcutaneously or intramuscularly, may also be used as a means to control and prolong the duration of action of a drug substance.[2] Most commonly, however, the poor aqueous solubility of drug candidates intended for oral administration constitutes a key challenge frequently leading to low and variable bioavailability of drugs.[3–5] Consequently, there is a demand for drug delivery approaches, which can increase drug exposure. Various enabling strategies have been pursued including supersaturating delivery systems utilizing the spring and parachute concept for improving drug bioavailability.[6,7] Arising from this is a significant interest around methods for characterizing supersaturation and precipitation events in a drug delivery context.[8,9] Solution concentration analysis is normally performed in an agitated system, evaluating the degree and duration of supersaturation of a drug substance or delivery system using UV-Vis spectrophotometry or high-performance liquid chromatography (HPLC) upon withdrawal of aliquots for analysis.[8,10] However, detection of precipitation is also of interest. Parameters such as, the onset of nucleation, particle size or solid state form are useful factors for ranking and evaluating supersaturating strategies.[9] Various techniques including light microscopy,[11,12] turbidity measurements,[13] UV-Vis absorbance-time measurements,[14,15] optical imaging[16,17] and Raman spectroscopy[16,18] are utilized to detect and monitor precipitation. The current methods for assessing supersaturation and precipitation phenomena are primarily applied to detect changes in a homogeneous solution environment and to monitor either the liquid or the solid phase. Therefore, methodologies where changes in both liquid and solid phases can be simultaneously followed upon precipitation are of value.

Here, we present our initial results obtained using a multimodal approach integrating novel dual wavelength UV-Vis imaging instrumentation with light microscopy and Raman spectroscopy to investigate the interplay between drug supersaturation, precipitation and dissolution in a flow-through setup in a non-homogeneous solution environment. UV imaging is the spatially and temporally resolved absorbance mapping.[19,20] Applying a selected wavelength in the UV range concentration distributions and, hence, drug dissolution and release processes have rendered possible, e.g., [21]. To initially investigate the potential of this platform allowing simultaneous imaging at two wavelengths, we developed a setup where the model drug, piroxicam dissolved in 1-methyl-2-pyrrolidinone, was introduced into an aqueous environment, and subject to precipitation due to solvent shift. Imaging at 405 nm, a wavelength where piroxicam absorbs light, provided information on piroxicam concentrations spatially and temporally resolved whereas the additional measurements using light obscuration (imaging at 525 nm), light microscopy

and Raman spectroscopy provided information on the behavior of precipitated particles in terms of formation, growth, dissolution and solid state.

Experimental section

Materials. N-Methyl-2-pyrrolidinone (NMP), piroxicam (P5654, anhydrate form) and phosphate buffered saline (PBS) tablets (P4417) were obtained from Sigma-Aldrich (St. Louis, MO, USA). Piroxicam monohydrate was prepared by adding deionized water and ethanol to piroxicam and leaving it overnight for the monohydrate to form under stirring. The solid was filtered off and dried. Milli-Q water was used throughout.

Dissolution medium and samples. Phosphate buffered saline (0.01 M phosphate buffer, 0.0027 M potassium chloride and 0.137 M sodium chloride; PBS), pH 7.4, was used as dissolution medium and was prepared by dissolving a PBS tablet in 200 ml of water. Sample solutions of piroxicam in NMP were prepared by dissolving piroxicam anhydrate in NMP at concentrations of 10 and 20 mg/ml (corresponding to 0.03 and 0.06 M piroxicam, respectively).

Cell design. The flow-through cell used for UV-Vis imaging, light microscopy and *in situ* Raman spectroscopy experiments was made from two quartz plates with dimensions of 75 × 26 × 1.0 mm^3 (L × W × D) (AdValue Technology, Tucson, AZ, USA) serving as top and bottom layer, separated by a 3D-printed support fabricated using a 3D desktop printer (MakerBot Replicator 2, MakerBot Industries, Brooklyn, USA) and Innofill polylactic acid (PLA) filaments with a diameter of 1.75 mm (Innofill^{3D} BV, Emmen, The Netherlands) (Fig. 1). This 3D-printed support provided the walls of the flow-through cell with inner dimensions of 40 × 21 × 4.0 mm^3 (L × W × D). The quartz plates were clamped to the flow-through cell to form a leak tight compartment when flow was applied. The flow-through cell contained an inlet and an outlet to realize a continuous flow of dissolution medium. An additional inlet was made to allow insertion of an 18G blunt needle (1.2 mm (OD) × 40 mm (length), Terumo, Leuven, Belgium) to introduce the piroxicam–NMP solutions into the cell. Two syringe pumps (a Fusion 200, Chemyx Inc., Stanford, TX, USA and a KDS-100-CE, KD Scientific, Holliston, MA, USA) were used to deliver the dissolution medium and drug solutions at constant rates.

UV-Vis imaging-based setup. The flow-through cell was integrated with an ActiPix D200 UV-Vis imaging system (Paraytec Ltd, York, UK) having an 11 × 11 mm^2 (H × W) CMOS chip and single pixel size of 5.5 × 5.5 μm^2. Dual wavelength imaging was performed using two LEDs at 405 nm and 525 nm. Images were recorded at a rate of 1 frame per second using the ActiPix D100 software from Paraytec Ltd (version 2.0.60330). Light intensities were converted into absorbance utilizing the ActiPix software.

Precipitation and dissolution studies. PBS and piroxicam in NMP solution were infused at rates of 5 ml/min (corresponding to linear flow rate of 1 mm/s) and 5 µl/min, respectively, at ambient temperature while UV-Vis images were recorded. The time for infusion of the piroxicam solutions was set at 2 min, while the infusion of the dissolution medium continued for an additional 8 min. A USB2000 UV–Vis spectrophotometer (Ocean Optics B.V, Duiven, The Netherlands) holding a flow-through cuvette (type 178.712-QS, 1 cm light path, Hellma GmbH & Co. KG, Müllheim, Germany) was employed to record the UV-Vis spectrum (200-800 nm) of the effluent every 30 s.

In parallel to UV-Vis imaging, a digital light microscope (Dino-Lite Premier Digital microscope, AM7013MZT, AnMo Electronics Corporation, Taiwan) was used to visualize piroxicam precipitation (40 × magnification) as shown in Fig. S-1. The solid form of the precipitated material was characterized in situ using a Raman RXN1 spectrometer with a PhAT probe (Kaiser Optical Systems, Ann Arbor, MI, USA). The spectrometer was equipped with a 785 nm Invictus laser with a power of approximately 200 mW. Spectra with a resolution of 5 cm^{-1} were obtained using Kaiser HOLOgrams software (Kaiser Optical Systems). Raman spectra were collected at times 30 s, 2 min, 6 min and 10 min after infusion of the piroxicam solution into the flow cell, which was placed on the microscope stage of the Raman spectrometer, with 1 s exposure time and 1 s accumulation. Reference Raman spectra of piroxicam anhydrate and piroxicam monohydrate powders were collected for comparison.

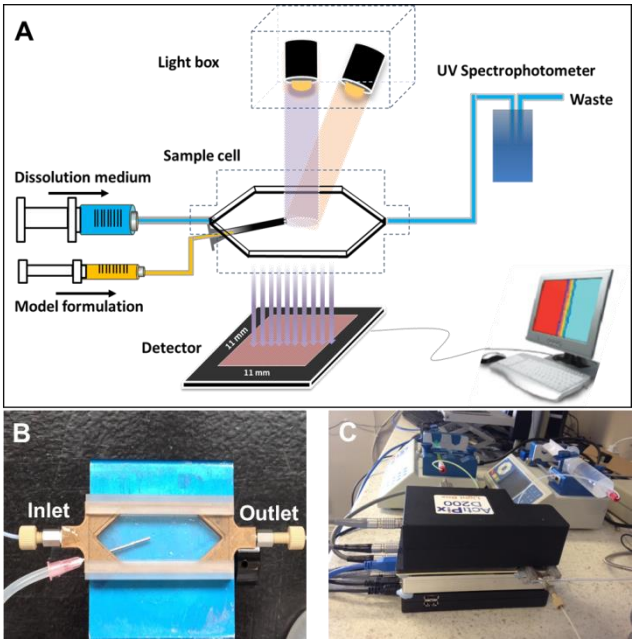

Figure 1. (A) Schematic representation of the UV-Vis imaging experimental setup. (B) Photograph (top view) of the flow-through cell (40 × 21 × 4.0 mm^3 (L × W × D)). (C) Photograph of the ActiPix D200 UV-Vis imaging system integrated with the flow-through cell.

Results and discussions

The thermodynamic solubility of piroxicam in NMP and PBS (pH 7.4) was determined to be $6.4 \cdot 10^{-1} \pm 1 \cdot 10^{-2}$ M and $1.20 \cdot 10^{-3} \pm 4 \cdot 10^{-5}$ M at 25 °C, respectively (cf. the Supporting Information). As might be expected from the difference in the solubility, piroxicam precipitated from a supersaturated solution upon the exchange of NMP and buffer solution. The behavior of piroxicam upon infusion of 10 µl 0.06 M piroxicam in NMP solution into flowing PBS was followed in real-time (a movie clip can be found in the Supporting Information Video S-1). Fig. 2 shows selected images obtained at 405 nm and 525 nm. The UV-Vis absorbance spectrum in Supporting Information Fig. S-2 shows that piroxicam dissolved in PBS absorbs light at 405 nm whereas it does not absorb at 525 nm. Initially, a detection wavelength of 280 nm where piroxicam exhibits a molar absorption coefficient of 13.2×10^3 M^{-1} cm^{-1}

higher than that at 405 nm (2.04×10^3 M^{-1} cm^{-1}) was selected for measuring the piroxicam concentration in the cell. However, results indicated that UV imaging of piroxicam at 280 nm was less suitable as the absorbance values obtained upon infusion of the concentrated solutions exceeded the working range

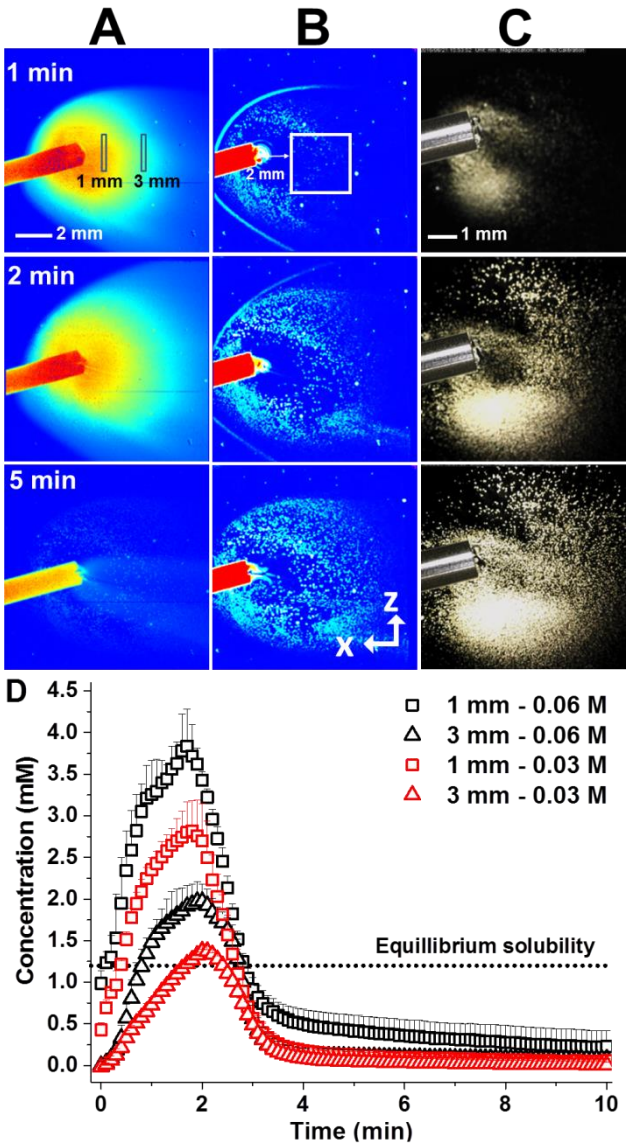

Figure 2. Time-dependent false-color images of absorbance along the x- and z-directions within an 11 × 11 mm^2 area of the flow cell at (A) 405 nm and (B) 525 nm as well as (C) light microscopy images obtained in a parallel study showing piroxicam precipitation and dissolution upon a 2 min injection of 10 µl 0.06 M piroxicam in NMP solution into the flowing phosphate buffered saline, pH 7.4. The flow direction was from left to right and the flow rate was 5 ml/min. For Figs. 2A and B, red color indicates high absorbance, while the blue color indicates low absorbance. The observed spatial displacement of the needle in Figs. 2A and B was due to the different positioning of the two LEDs in the light box as indicated in Fig. 1A. (D) Piroxicam concentration-time profiles at specific distances from the needle tip upon injection of 10 µl 0.03 M and 0.06 M piroxicam in NMP solution (n = 3). The concentrations were determined from the averaged absorbance measured in the two 0.02 × 2 mm^2 areas, indicated by the black squares, placed at 1 mm and 3 mm from the needle tip in the absorbance maps at 405 nm of Fig. 2A.

of the detector in the vicinity of the needle tip. Consequently, a wavelength of 405 nm was chosen for the following studies. The wavelength of the D200 imaging system is from 200 nm to 800 nm depending on the LEDs and filters selected for the system.

The images at 525 nm revealed piroxicam precipitation and light scattering from piroxicam particulates. The absorbance at 405 nm was obtained as a result of molecularly dissolved piroxicam as well as light obscuration (absorbance and scattering) from particulates. As seen from the images at 525 nm (Fig. 2B), piroxicam precipitation occurred almost instantaneously upon initiation of the infusion of the 0.06 M piroxicam in NMP solution. From Fig. 2, it is evident that the continuous infusion (first 2 min) of 0.06 M piroxicam in NMP solution resulted in a gradual increase in piroxicam absorbance and concentration (Fig. 2A) as well as in the number of the precipitated particles (Fig. 2B). Upon termination of the infusion of piroxicam, the absorbance at 405 nm due to piroxicam dissolved or in suspension in the cell decreased due to removal in the PBS flow (Fig. 2A at 5 min). However, continued precipitation, predominantly in the proximity of the needle tip (Fig. 2B at 5 min) was observed. The absorbance maps at 405 nm were converted into piroxicam concentration maps using a calibration curve covering the range of 0.1 - 3.6 mM piroxicam in PBS (Fig. S-3). It is known that piroxicam is capable of forming supersaturated solutions.[22] The standard solutions were prepared by dilution of a stock solution of 10 mM piroxicam in NMP. The calibration curve covered concentrations above the piroxicam solubility in PBS. These supersaturated solutions were sufficiently stable allowing the construction of the calibration curve in the flow-through setup. Thus, it was possible to detect and quantify piroxicam concentration distribution in the cell. Fig. 2D depicts the apparent piroxicam concentration for a selected area within the images as a function of time for the infusion experiments. UV-Vis imaging is in essence a 2D technique, and the images clearly reveal concentration distributions over the image area in the xz plane. However, it should be appreciated that the absorbance values read are averaged over the light path through the flow-through cell (the y axis) where concentration gradients also must be anticipated. Consequently, the piroxicam concentrations reported should be considered as apparent concentrations, which is emphasized by the fact that when converting the volume of the infused piroxicam solution 10 µl to a perfect sphere, the corresponding sphere has a radius of 1.34 mm, which can be compared to the 4 mm light path of the flow cell. Upon infusion of the solution of 0.06 M piroxicam in NMP, precipitation occurred almost immediately. By contrast, significantly less precipitation was detected by UV-Vis imaging for the first minute when infusing the solution of 0.03 M piroxicam in NMP (Supporting Information Fig. S-4 and Video S-2). Qualitatively, these findings were expected since a higher piroxicam concentration promotes a higher degree of supersaturation facilitating rapid nucleation and precipitation. The apparent levels of supersaturation achieved by the two piroxicam in NMP solutions are depicted in Fig. 2D. The concentration-time profiles shown in Fig. 2D were determined by averaging the absorbance over 0.02 × 2 mm areas positioned at distances of 1 and 3 mm from the needle tip and indicated by the squares in Figs. 2A and S-4A. For both solutions, local supersaturation conditions endured for approximately 2 min, reaching apparent concentration levels of 3.8 mM and 2.8 mM for the solutions of 0.06 M and 0.03 M piroxicam in NMP, re

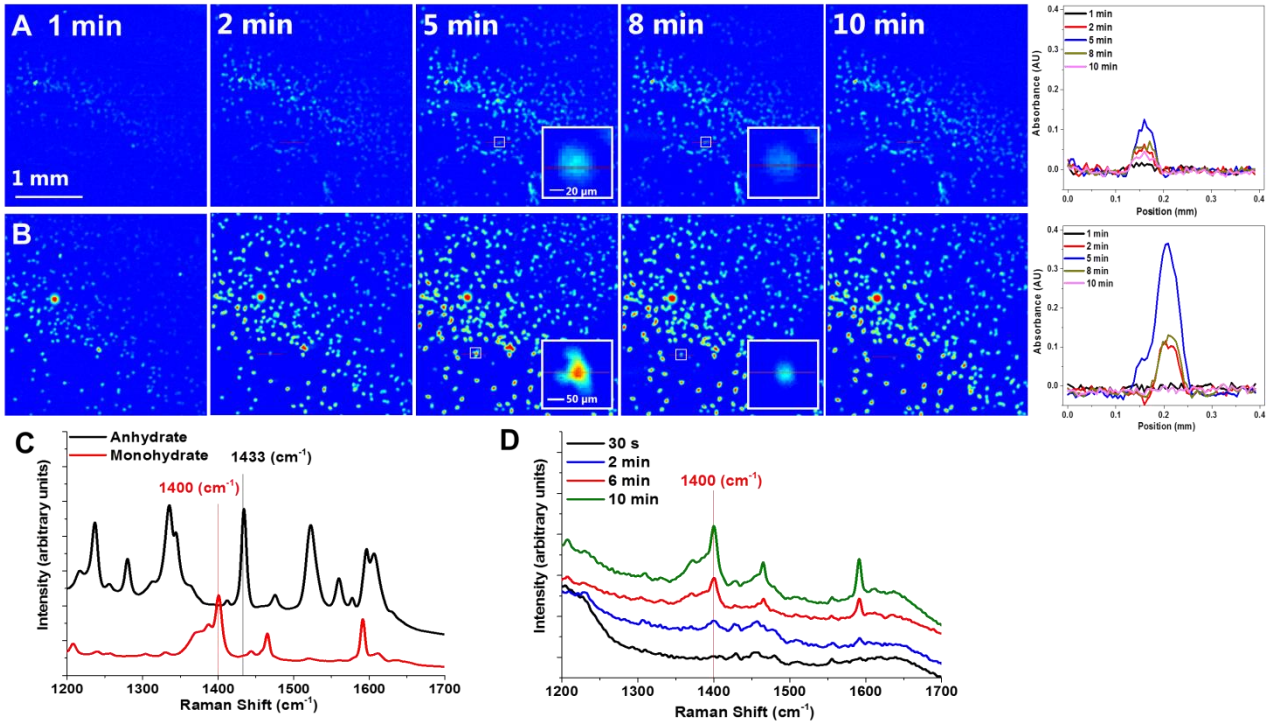

Fig. 3. Selected areas of 3 × 3 mm^2 from absorbance maps obtained at 525 nm corresponding to the white squares in Figs. 2B and S-4, showing formation and dissolution of piroxicam particles as a function of time upon injection of 10 µl (A) 0.03 and (B) 0.06 M piroxicam in NMP solution into the flowing phosphate buffered saline, pH 7.4 (5 ml/min). Insets are the zoom-in images of a selected piroxicam particle subjected to study. The last column presents the time-dependent absorbance-position (z, mm) profiles at 525 nm along the red lines overlaid the selected particles. (C) Reference Raman spectra and (D) sample spectra as a function of time for 0.06 M piroxicam in NMP solution.

spectively, at the region 1 mm downstream from the needle tip. The differences with respect to apparent local piroxicam concentration and extent of precipitation detected by UV-Vis imaging after introduction of 0.03 M and 0.06 M piroxicam solutions were consistent with light microscopy images (Fig. 2C and Fig. S-4C). The different behavior of piroxicam upon infusion at the two concentrations was further corroborated by downstream UV spectrophotometry (Fig. S-5). For solutions containing 0.06 M piroxicam in NMP, the extensive precipitation and sedimentation of piroxicam in the cell led to a significantly smaller fraction of the infused piroxicam recovered in the effluent as compared to the recovery upon infusing 0.03 M piroxicam in NMP solutions under similar conditions. The amounts of piroxicam infused were 0.60 µmol and 0.30 µmol and the cumulative amounts recovered by downstream UV spectrophotometry after 10 min were 0.38 ± 0.04 µmol and 0.31 ± 0.01 µmol, respectively.

In contrast to most precipitation assays, the concentration distribution was not homogenous because of the flow cell design and non-laminar flow conditions, which were revealed by the UV images (data not shown). Also, the orientation of the flow cell had a substantial effect on the observed precipitation behavior of piroxicam. Using the flow-through cell in the horizontal orientation depicted in Fig. 1 led to particles precipitating and settling on the lower quartz plate within the imaging area, whereas positioning the flow-through cell in an upright orientation led to a narrow stream of piroxicam in NMP transported from the needle without apparent broadening over an imaging distance of ~ 5 mm (Supporting Information Fig. S-6). Only a few particles were observed within the imaging region using this latter configuration. These differences may be correlated to the different hydrodynamic and mixing conditions prevailing utilizing the two configurations. In the former case, natural convection due to density differences forces the NMP solution, which is more dense than PBS, towards the bottom quartz plate where a lower flow velocity will be experienced due to the limited height of the flow cell (4 mm with 0.84 mm ID needle placed in the middle). This apparently leads to an environment facilitating the precipitation of piroxicam (Fig. 2). In the latter case, there will only be a limited change in flow velocity due to density effects because the effective height of the cell using this orientation is 21 mm. The average linear flow velocity during infusion of the NMP solution at the needle tip and the average bulk flow linear velocity of the flow cell can be estimated to 9.0 mm min^{-1} and 60 mm min^{-1}, respectively. These flow rates may be used in support of the notion that the PBS provides a sheath flow surrounding the NMP flow stream and thereby limiting mixing and precipitation in the so-called upright position as apparent from Fig. S-6. To this end, the density of solid piroxicam has been reported to be 1.481 g cm^{-3};[23] for 0.06 M piroxicam in NMP and for the PBS densities of 1.038 g cm^{-3} and 1.005 g cm^{-3}, respectively, were determined at 20 °C (cf. Supporting Information). The observations are consistent with previous UV imaging based studies, which revealed the importance of density gradients for the dissolution of lidocaine.[24] Overall the supersaturation, precipitation and dissolution processes occurring remain the same in the studies performed, however, the sensitivity of the processes to changes with respect to geometry an hydrodynamics is efficiently captured by UV-Vis imaging as highlighted in Fig. 2, Fig. S-4 and Fig. S-6.

The extent of precipitation as well as the form in which a drug substance precipitates may be of importance, e.g., for oral bioavailability.[6,7,9,15] Figs. 2 and S-4 document the relation between the extent of precipitation and the degree of supersaturation. Expansion of the images in the time-dependent sequences in the horizontally-mounted flow cell at 525 nm reveals further details. Figs. 3A and B show the appearance, growth in size and subsequent dissolution of piroxicam particles. For the measurement times, 1, 2, 5, 8 and 10 min, both individual particles visualized showed maximum absorbance (size) around 5 min. This pattern of precipitation, growth and dissolution was found for both piroxicam solutions. However, the timing of the events for the individual particles was found to be concentration and position dependent. The solid state form of the piroxicam particles forming during the experiments was identified by *in situ* Raman spectroscopy upon positioning the flow cell on the microscope stage of the Raman spectrometer. It was possible to obtain a good Raman signal from the piroxicam particles precipitated from 0.06 M piroxicam in NMP solution under flow conditions. Raman spectroscopy (Figs. 3C and D) revealed that piroxicam precipitated as the monohydrate form. Here Raman spectroscopy was applied for asserting the form in which piroxicam precipitated. The setup may have potential for monitoring potential solid form transformations. Quantitative assessment of the precipitation kinetics from the Raman spectra as has been done by Arnold *et al*.[16] in a homogenous solution/suspension environment will be challenging.

CONCLUSIONS

Dual-wavelength imaging provides an approach for simultaneous characterization of piroxicam supersaturation, precipitation and dissolution during piroxicam precipitated from a piroxicam-NMP solution in a flow-through setup. The open design of the flow-through cell, with large area quartz windows suitable for visualization of the interaction between flow streams of sample solution and anti-solvent, allowed detailed investigation of drug precipitation and dissolution events using UV-Vis imaging, light microscopy and Raman spectroscopy. Such a combination of analytical techniques may be advantageous for attaining a thorough understanding of drug precipitation and dissolution processes in various systems. In the future, this proof-of-principle setup may be further developed to characterize the performance of supersaturating, *in situ* forming and particulate drug delivery systems. The ability to fabricate flow cell bodies using 3D printing and the ability to mount the cell together with the light source and imaging modules in different orientations provide~~s~~ a lot of flexibility for exploration of various hydrodynamic conditions. Refinement with respect to image analysis is needed to further improve the versatility of the setup. In a broader perspective, the developed approach may potentially serve as a tool in formulation screening and development.

ASSOCIATED CONTENT

Supporting Information

The Supporting Information is available free of charge on the ACS Publications website.

Supporting experimental section and supporting figures (PDF)

Video clips of precipitation – dissolution experiments (AVI)

AUTHOR INFORMATION

Corresponding Author

***** Jesper Østergaard

Department of Pharmacy, Faculty of Health and Medical Sciences, University of Copenhagen, Universitetsparken 2, DK-2100 Copenhagen Ø, Denmark.

Tel.: +45 35336138; fax: +45 35336030.

E-mail address: jesper.ostergaard@sund.ku.dk

Notes

Paraytec Ltd. (York, UK) develops and manufacturers UV imaging instrumentation. Jesper Østergaard is member of the Scientific Advisory Board of Paraytec Ltd.

ACKNOWLEDGMENT

This project has received funding from the European Union's Horizon 2020 research and innovation program under the Marie Sklodowska-Curie grant agreement No 644056. The authors alone are responsible for the content and writing of this paper.

REFERENCES

(1) Yalkowsky, S. H.; Krzyzaniak, J. F.; Ward, G. H. *J. Pharm. Sci.* **1998**, *87* (7), 787–796.
(2) Packhaeuser, C. .; Schnieders, J.; Oster, C. .; Kissel, T. *Eur. J. Pharm. Biopharm.* **2004**, *58* (2), 445–455.
(3) Pouton, C. W. *Eur. J. Pharm. Sci.* **2006**, *29* (3), 278–287.
(4) Stegemann, S.; Leveiller, F.; Franchi, D.; de Jong, H.; Lindén, H. *Eur. J. Pharm. Sci.* **2007**, *31* (5), 249–261.
(5) Gupta, S.; Kesarla, R.; Omri, A. *ISRN Pharm.* **2013**, *2013*, 1–16.
(6) Brouwers, J.; Brewster, M. E.; Augustijns, P. *J. Pharm. Sci.* **2009**, *98* (8), 2549–2572.
(7) Liu, C.; Chen, Z.; Chen, Y.; Lu, J.; Li, Y.; Wang, S.; Wu, G.; Qian, F. *Mol. Pharm.* **2016**, *13* (2), 599–608.
(8) Bevernage, J.; Brouwers, J.; Brewster, M. E.; Augustijns, P. *Int. J. Pharm.* **2013**, *453* (1), 25–35.
(9) Dai, W. *Int. J. Pharm.* **2010**, *393* (1–2), 1–16.
(10) Palmelund, H.; Madsen, C. M.; Plum, J.; Müllertz, A.; Rades, T. *J. Pharm. Sci.* **2016**, *105* (10), 3021–3029.
(11) Raghavan, S. L.; Kiepfer, B.; Davis, A. F.; Kazarian, S. G.; Hadgraft, J. *Int. J. Pharm.* **2001**, *221* (1), 95–105.
(12) Wu, J. X.; Xia, D.; van den Berg, F.; Amigo, J. M.; Rades, T.; Yang, M.; Rantanen, J. *Int. J. Pharm.* **2012**, *433* (1–2), 60–70.
(13) Morrison, J. S.; Nophsker, M. J.; Haskell, R. J. *J. Pharm. Sci.* **2014**, *103* (10), 3022–3032.
(14) Bernardo, A.; Calmanovici, C. E.; Miranda, E. A. *Cryst. Growth Des.* **2004**, *4* (4), 799–805.
(15) Ozaki, S.; Minamisono, T.; Yamashita, T.; Kato, T.; Kushida, I. *J. Pharm. Sci.* **2012**, *101* (1), 214–222.
(16) Arnold, Y. E.; Imanidis, G.; Kuentz, M. T. *J. Pharm. Pharmacol.* **2011**, *63* (3), 333–341.
(17) Evans, D. C.; Kudenov, M. W.; Sassenrath, K. C.; Dereniak, E. L.; Yalkowsky, S. H. *Int. J. Pharm.* **2016**, *512* (1), 219–223.
(18) Raut, S.; Karzuon, B.; Atef, E. *J. Pharm. Biomed. Anal.* **2015**, *109*, 121–127.
(19) Østergaard, J.; Meng-Lund, E.; Larsen, S. W.; Larsen, C.; Petersson, K.; Lenke, J.; Jensen, H. *Pharm. Res.* **2010**, 27, 2615-2623.
(20) Østergaard, J.; Wu, J. X.; Naelapää, K.; Boetker, J. P.; Jensen, H.; Rantanen, J. *J. Pharm. Sci.* **2014**, *103*, 1149-1156.
(21) Østergaard, J. *J. Pharm. Biomed. Anal.* **2018**, *147*, 140-148.
(22) Pellett, M. A.; Castellano, S.; Hadgraft, J.; Davis, A. F. *J. Control. Release* 1997, 46 (3), 205–214.

(23) Kojić-Prodić, B.; Ružić-Toroš, Ž. *Acta Crystallogr. B* **1982**, *38* (11), 2948–2951.
(24) Østergaard, J.; Ye, F.; Rantanen, J.; Yaghmur, A.; Larsen, S. W.; Larsen, C.; Jensen, H. *J. Pharm. Sci.* 2011, *100*, 3405-3410.

TOC graphic: